

# Survey of the ISM in Early-Type Galaxies. IV. The Hot Dust Component <sup>\*</sup>

F. Ferrari<sup>1</sup>, M.G. Pastoriza<sup>1</sup>, F.D. Macchetto<sup>2,3</sup>, C. Bonatto<sup>1</sup>, N. Panagia<sup>2</sup>, and W. B. Sparks<sup>2</sup>

<sup>1</sup> Instituto de Física, UFRGS, Porto Alegre, Brazil

<sup>2</sup> Space Telescope Science Institute

<sup>3</sup> On assignment from the Space Science, Department of ESA

Received date, Accepted 2002 April 16

**Abstract.** We present mid-IR photometric properties for a sample of 28 early-type galaxies observed at 6.75, 9.63 and 15  $\mu\text{m}$  with the ISOCAM instrument on board the ISO satellite. We find total mid-IR luminosities in the range  $3 - 48 \times 10^8 L_{\odot}$ . The spectral energy distribution (SED) of the galaxies were derived using the mid-IR data together with previously published UV, optical and near-IR data. These SEDs clearly show a mid-IR emission coming from dust heated at  $T \simeq 260$  K. Dust grains properties are inferred from the mid-IR colors. The masses of the hot dust component are in the range  $10 - 400 M_{\odot}$ . The relationship between the masses derived from mid-IR observations and those derived from visual extinction are discussed. The possible common heating source for the gas and dust is investigated through the correlations between  $H\alpha$  and mid-IR luminosities.

**Key words.** galaxies: early-type, interstellar medium

## 1. Introduction

The presence and properties of the interstellar medium (ISM) in early-type galaxies have been the subject of intense work in the last decades. In particular, dust lanes and patches have been detected in a large fraction of such galaxies, typically in about 75% of the objects. The morphology of the dust distribution in these galaxies follows very closely that of the ionized gas (Ferrari et al. 1999, Goudfrooij et al. 1994a) and typical dust masses in the range  $10^3 - 10^5 M_{\odot}$  have been found (Ferrari et al. 1999; Goudfrooij et al. 1994b). These results were confirmed also by optical HST data, which showed that 78% of the early-type galaxies contain nuclear dust (Van Dokkum & Franx 1995). However, dust masses derived from the IRAS flux densities (Knapp et al. 1989) are found to be roughly an order of magnitude higher than those derived from the optical extinction values. This is in strong contrast with what is found in spiral galaxies where dust masses derived from the optical extinction and IRAS luminosities are in agreement (Goudfrooij et al. 1995, Merluzzi 1998). To account for this difference it was argued that most of the

dust in elliptical galaxies exists as a diffuse component essentially undetectable at optical wavelengths. This diffuse dust component produces a radial color gradient that adds to the gradient produced by metallicity and stellar population age, as shown by Goudfrooij & Jong (1995).

Knowledge of the ISM dust emission properties in galaxies has greatly increased over the last years due to the ISO satellite which has provided high quality data in the spectral range  $3 - 200 \mu\text{m}$ . The IR emission of the interstellar medium of galaxies is mainly due to dust heated by the interstellar radiation field and a large fraction of this emission is observed in the near and mid-IR. The emission in this region has been explained under the hypothesis of a dust population formed by very small ( $a < 0.02 \mu\text{m}$ ) grains with a fluctuating temperature, due to the absorption of individual UV photons. Emission in the wavelength range  $3 < \lambda < 15 \mu\text{m}$  is also produced by Unidentified Infrared Emission Bands (UIBs) associated with the Polycyclic Aromatic Hydrocarbons (PAHs) (Desert et al. 1990). The mid-IR emission of a selected sample of Virgo cluster early-type galaxies has been studied by Boselli et al. (1998), who concluded that the emission up to  $15 \mu\text{m}$  is dominated by the Rayleigh-Jeans tail of the old stellar population. A survey of a larger number of E and SO galaxies using broad band filter ISOCAM imaging covering the range  $4.5$  to  $18 \mu\text{m}$  shows that dust present in the form of small hot grains and/or UIB also contributes to the mid-IR emission in these galaxies (Madden et al. 1999).

Send offprint requests to: Fabricio Ferrari, e-mail: ferrari@if.ufrgs.br

<sup>\*</sup> Based on observations with ISO, an ESA project with instruments founded by ESA member states (especially the PI countries: France, Germany, the Netherlands and the United Kingdom) and with participation of ISAS and NASA.

The origin of the gas and dust in early-type galaxies is still a highly controversial subject. Alternative scenarios include a normal quiescent component, accretion by merger events and cooling flows (Sparks et al. 1989, Kim 1989, Fabian 1994). In order to contribute to the investigation of the ISM origin in early-type galaxies, we have carried out an extensive program of imaging and spectroscopy of a large sample of bright E and S0 galaxies. The ionized gas properties in these galaxies are discussed in Macchetto et al. (1996, hereafter Paper I). The morphology of the dust distribution and the optical absorption  $A_V$  together with assumptions on dust grain composition allowed us to estimate the dust masses for the galaxy sample. These results were presented in Ferrari et al. (1999, hereafter Paper II). Gas and star kinematics for 12 of these galaxies are discussed in Caon et al. (2000).

In the present paper we discuss the properties of the mid-IR emission in 28 early-type galaxies observed with the ISOCAM instrument on board the ISO Satellite for which we have obtained broad band imaging, covering the range 5 to 18  $\mu\text{m}$ . For each galaxy we have estimated the total mid-IR luminosity, mid IR colors and dust properties. We have compared these results with those inferred from the optical absorption and explored the correlation between the mid-IR dust luminosity with the ionized gas luminosity given in Paper I and dust masses derived from optical data from Paper II.

This paper is structured as follows: in Section 2 we present the galaxy sample; in Section 3 we discuss the observations and data reduction. The Spectral Energy Distributions of the target galaxies are derived in Section 4. The luminosity distribution at the three observed frequencies is presented in section 5, and mid-IR colors in Section 6. Dust mass estimates from the mid-IR observations are presented in Section 7. Finally, the conclusions are given in Section 8.

## 2. The sample

The objects studied in this paper, extensively described in Papers I and II, are luminous galaxies ( $B_T < 13$ ) with morphological types E and SO selected from “The Reference Catalog of Bright Galaxies” (RC3) to provide a fairly large interval in optical luminosity including both radio-loud and radio-quiet galaxies, X-ray emitters and non-emitters. A large fraction of the galaxies in this sample (72%) contains ionized gas (Paper I) and considerable amounts of dust (Paper II). This sample is not complete in any sense, rather it includes rich ISM galaxies. 14 galaxies have IRAS upper limits only; 8 were detected in 2 IRAS bands and have 2 upper limits and only 3 have reliable IRAS data. Our sample galaxies are listed in Table 1 along with their coordinates, morphological type, magnitudes, distances and stellar population groups (discussed later).

Distances have been derived with the “220 model” for the Virgo Infall of Kraan-Korteweg (1986) assuming the Virgo Cluster at a distance of 21.3 Mpc. For galaxies not

present in the Kraan-Korteweg’s list, distances were derived from their redshift corrected to the reference frame defined by the cosmic microwave radiation (from RC3). All distances were then rescaled according to the value of  $H_0 = 65 \text{ Km s}^{-1} \text{ Mpc}^{-1}$  (Macchetto et al. 1999).

## 3. Observations and data reductions

The observations were carried out with the  $32 \times 32$  element infrared camera (ISOCAM) on board the ISO satellite. ISOCAM was used to perform a raster image covering the central body of the targets. The raster was built by combining the individual frames (usually more than 100 in each target) slightly shifted along the observation. The final raster has  $36 \times 36$  pixels, or  $108'' \times 108''$ , since the pixel field of view (PFOV) is  $3''$ . The single integration time was 7 sec in most cases. All galaxies were observed in 3 filters LW2 ( $\lambda_c = 6.75 \mu\text{m}$ ,  $\Delta\lambda = 2.5 \mu\text{m}$ ), LW3 ( $\lambda_c = 15.0 \mu\text{m}$ ,  $\Delta\lambda = 5 \mu\text{m}$ ) and LW7 ( $\lambda_c = 9.63 \mu\text{m}$ ,  $\Delta\lambda = 2 \mu\text{m}$ ). The ISOCAM data presented in this paper were analyzed using CIA<sup>1</sup>: the images were dark-subtracted, flat-fielded, deglitched, corrected for transient effects in the detector and combined to produce a final raster image. At first approach, we used the mid-IR sky model by Kelsall et al. (1998), however the resulting fluxes were too large compared with 12  $\mu\text{m}$  IRAS fluxes. Consequently, the sky background was measured in the galaxy frames. In some cases (NGC 720, NGC 4374, NGC4472, NGC 4636) the field of view is smaller than the size of the galaxy, which could lead to overestimated sky values and consequently underestimated galaxy fluxes for these galaxies.

The total fluxes were integrated in the raster images after removing the background and then converted to mJy using the conversion factor in the CIA packages. The absolute fluxes are estimated to be accurate to 30% due to ISO calibration errors (Cesarsky and Blommaert 2000). It should be mentioned that the ISOCAM fluxes ( $50 \leq F \leq 374 \text{ mJy}$ ) correspond to the range where the camera is quite sensitive and accurate. ISO total integrated fluxes inside the field of view as well as IRAS data are listed in Table 2. To test the reliability of ISOCAM data we made a comparison with IRAS 12 $\mu\text{m}$  data (Fig. 1). However, 12 $\mu\text{m}$  fluxes fall in a range corresponding to IRAS upper limit detection, consequently these values are not so reliable as ISOCAM fluxes. If we do not consider IRAS 12 $\mu\text{m}$  fluxes below  $\sim 60 \text{ mJy}$ , which are below the instrument detection limit, there is a good agreement between ISO 6.75 $\mu\text{m}$  and IRAS 12 $\mu\text{m}$  fluxes. The same for ISO 15 $\mu\text{m}$  and IRAS 12 $\mu\text{m}$  fluxes, except for two galaxies (NGC 4472 and NGC 4636) which are active galaxies. It can also be seen that ISO 9.63 $\mu\text{m}$  fluxes are systematically larger than IRAS 12 $\mu\text{m}$  fluxes and this may be due to the presence of some silicate bands that lie in the 9.63 $\mu\text{m}$  filter spectral region. Furthermore, we should

<sup>1</sup> CIA is a joint development by the ESA Astrophysics Division and the ISOCAM consortium. The ISOCAM consortium is led by the ISOCAM PI, C. Cesarsky.

Name	$\alpha(2000)$	$\delta(2000)$	Type	$B_T^0$	D (Mpc)	SED
NGC 720	01 52 57.5	-13 30 20	E5	11.16	25.4	-
NGC 741	01 56 21.0	+05 37 44	E0	12.2	84.0	-
NGC 1453	03 46 27.2	-03 58 09	E2	12.58	59.1	K7
NGC 3258	10 28 54.1	-35 36 22	E1	12.22	42.9	-
NGC 4374	12 25 03.7	+12 53 13	E1	10.01	15.8	K4
NGC 4472	12 29 46.8	+08 00 01	E2/S0	9.33	18.0	K4
NGC 4636	12 42 50.0	+02 41 17	E/S0	10.43	18.0	-
NGC 4783	12 54 36.3	-12 33 30	E0pec	12.80	71.2	-
NGC 4936	13 04 16.4	-30 31 29	E0	12.28	50.4	K7
NGC 5044	13 15 24.0	-16 23 06	E0	11.87	44.2	K7
NGC 5084	13 20 16.7	-21 49 39	S0	11.28	26.6	M0
NGC 5813	15 01 11.2	+01 42 08	E1	11.42	29.5	K4
NGC 5831	15 04 07.2	+01 13 15	E4	12.31	29.5	M0
NGC 5903	15 18 36.3	-24 04 06	E3/S0	11.74	37.5	K7
NGC 6407	17 44 57.7	-60 44 22	E	12.43	67.9	K4
NGC 6721	19 00 50.5	-57 45 28	E1	12.68	64.9	M0
NGC 6758	19 13 52.3	-56 18 33	E2	12.31	49.7	K7
NGC 6776	19 25 19.4	-63 51 41	E1pec	12.71	79.9	M0
NGC 6851	20 03 33.6	-48 17 02	E4	12.51	41.1	K4
NGC 6868	20 09 53.8	-48 22 45	E3/S0	11.49	41.1	K7
NGC 6876	20 18 20.3	-70 51 28	E3	11.83	57.4	-
NGC 7041	21 16 32.6	-48 21 51	S0/E7	12.19	27.7	K7
NGC 7562	23 15 57.7	+06 41 15	E2-3	12.38	51.9	M0
NGC 7619	23 20 14.7	+08 12 23	E	11.93	51.9	M0
NGC 7626	23 00 42.3	+08 13 02	Epec	12.06	51.9	-
NGC 7796	23 58 59.7	-55 27 23	E+	12.39	47.7	K4
IC 4889	19 45 15.8	-54 20 37	E5	12.06	36.8	-
IC 5105	21 24 22.4	-40 32 06	E+	12.62	79.1	M0

**Table 1.** Names, coordinates, morphological types, integrated total blue magnitudes and distances ( $H_0 = 65 \text{ km s}^{-1} \text{ Mpc}^{-1}$ ) for the galaxies in the sample. SED describes the color of the dominant stellar contribution (see text); - means galaxies not classified in any group.

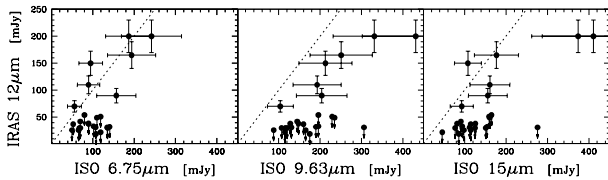


**Fig. 1.** Relation between ISO and IRAS data for the galaxy sample. The straight line represents the one-one correlation.

not expect ISOCAM and  $12\mu\text{m}$  IRAS fluxes to agree better than for a factor of 2, because of the differences in the field of view, filters sensitivity and bandpasses.

For most of the observed galaxies, the mid-IR emission is extended, although its distribution varies among the filters, probably due to the relative contribution of stars and dust in each filter. Figures 2, 3 and 4 present the isophotes of IC 4889, a typical example of our sample. The isophotes at  $6.75 \mu\text{m}$  are circular, corresponding to the dominant contribution of the galaxy stellar bulge, while at longer wavelengths, where the dust emission begins to dominate, the isophotes becomes more irregular. A general

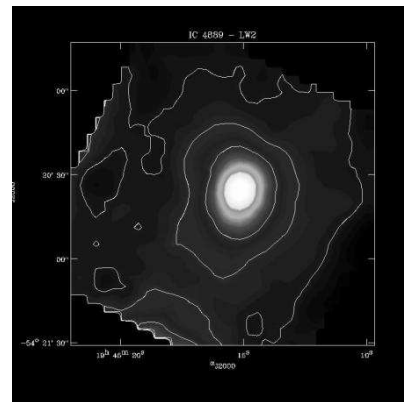


**Fig. 2.** LW2 ( $6.75 \mu\text{m}$ ) image of the IC 4889 galaxy.

feature of isophote maps is a concentration of dust around the optical nucleus of each galaxy.

#### 4. Spectral energy distributions

In order to estimate the relative contributions of the stellar component and dust emission to the mid-IR luminosity in early-type galaxies, we have built the spectral energy distribution (SED) for each galaxy using our ISOCAM

Galaxy	Total Fluxes			
	$6.75\mu\text{m}$ (mJy)	$9.63\mu\text{m}$ (mJy)	$15\mu\text{m}$ (mJy)	IRAS12 $\mu\text{m}$ (mJy)
NGC 720	157	204	156	90
NGC 741	65	209	61	—
NGC 1453	90	193	161	110
NGC 3258	53	160	115	< 37
NGC 4374	194	251	177	165
NGC 4472	242	331	374	200
NGC 4636	187	431	411	200
NGC 4783	70	145	91	< 42
NGC 4936	119	115	46	< 22
NGC 5044	95	213	108	150
NGC 5084	119	229	159	< 51
NGC 5813	136	116	151	< 30
NGC 5831	65	222	152	—
NGC 5903	80	196	165	< 54
NGC 6407	90	128	82	< 38
NGC 6721	50	165	115	< 26
NGC 6758	56	104	93	70
NGC 6776	68	107	77	< 30
NGC 6851	90	148	126	< 38
NGC 6868	141	190	154	< 32
NGC 6876	125	192	107	—
NGC 7041	135	306	276	< 31
NGC 7562	107	131	112	< 31
NGC 7619	102	196	94	< 33
NGC 7626	110	235	161	< 49
NGC 7796	108	175	86	< 19
IC 4889	70	121	125	< 30
IC 5105	66	88	98	< 26

**Table 2.** Total integrated fluxes inside the field of view for the galaxies in the sample.

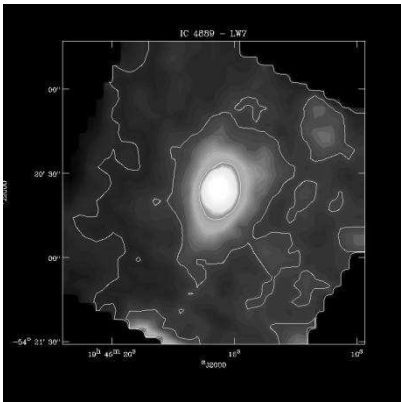


**Fig. 3.** LW7 ( $9.63\mu\text{m}$ ) image of the IC 4889 galaxy.

data together with UV, optical, near and IRAS IR data taken from the NASA Extragalactic Database<sup>2</sup>. We have taken from NED the optical and near-IR magnitudes integrated inside an aperture similar to that corresponding

<sup>2</sup> The NASA/IPAC Extragalactic Database (NED) is operated by the Jet Propulsion Laboratory, California Institute of Technology, under contract with the National Aeronautics and Space Administration

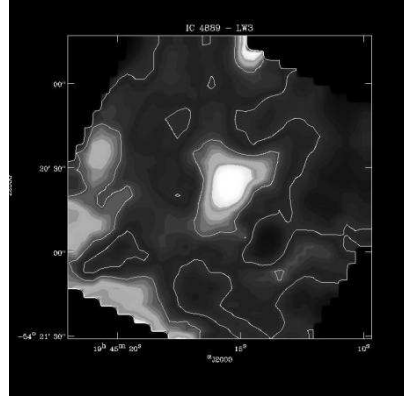


**Fig. 4.** LW3 ( $15\mu\text{m}$ ) image of the IC 4889 galaxy.

to the ISOCAM field of view ( $108''$ ). UV and IRAS data are total integrated values. Some IRAS values (black dots in Figures 5, 6, 7 and 8) are upper limits. All fluxes were normalized to the near-IR K magnitude. We then superposed black body (BB) curves to each galaxy SED and found that the UV, optical and near-IR data for all galaxies can be well matched with BBs of three different temperatures  $T=3750\text{ K}$ ,  $T=4000\text{ K}$  and  $T=4600\text{ K}$ . These temperatures correspond to dominant stellar populations of spectral types M0, K7 and K4, respectively. The mid-IR data have been fitted ( $\chi^2$ ) with a composite BB curve  $B_\nu(T) Q_\nu = B_\nu(T) \nu^{1.6}$  for isothermal grains (Natta & Panagia 1976) with  $T=260\text{ K}$ , for which the hot dust is an important contributor. For more than 30% of the galaxies in the sample there are no published near-IR observations, therefore to normalize the SED to the K band, we have estimated the K flux from the BB curve which fits the observed UV and optical data. This normalization was not applied to the BB with  $T=260\text{ K}$  because at this temperature the K flux is too small and the normalization would produce high mid-IR values for the BB. Besides, we are interested in the color temperature rather than in absolute fluxes. The SED for each galaxy is shown in Fig. 5 along with the corresponding BB curves for the stellar population and dust. There is a remarkable uniformity among the galaxies with respect to the dust emission properties, except for NGC 720, NGC 4374, NGC 4472 and NGC 4636 whose sizes are much greater than ISOCAM FOV, leading to underestimated fluxes. We have arranged the galaxy SEDs in three different groups named M0, K7 and K4, which are shown in Figures 6 to 8, according to the effective temperature of the stellar population that represents its SED. Together with the data points we have plotted black body radiation curves to illustrate the stellar population contribution in comparison with the dust component.

It is interesting to stress that all SEDs of our elliptical galaxies are fitted from the UV to the mid-IR with only two components, one representing the dominant stellar population continuum and the other the hot dust emission. The dust component is remarkably uniform in temperature for all the sample,  $T \simeq 260\text{ K}$ . We will there-

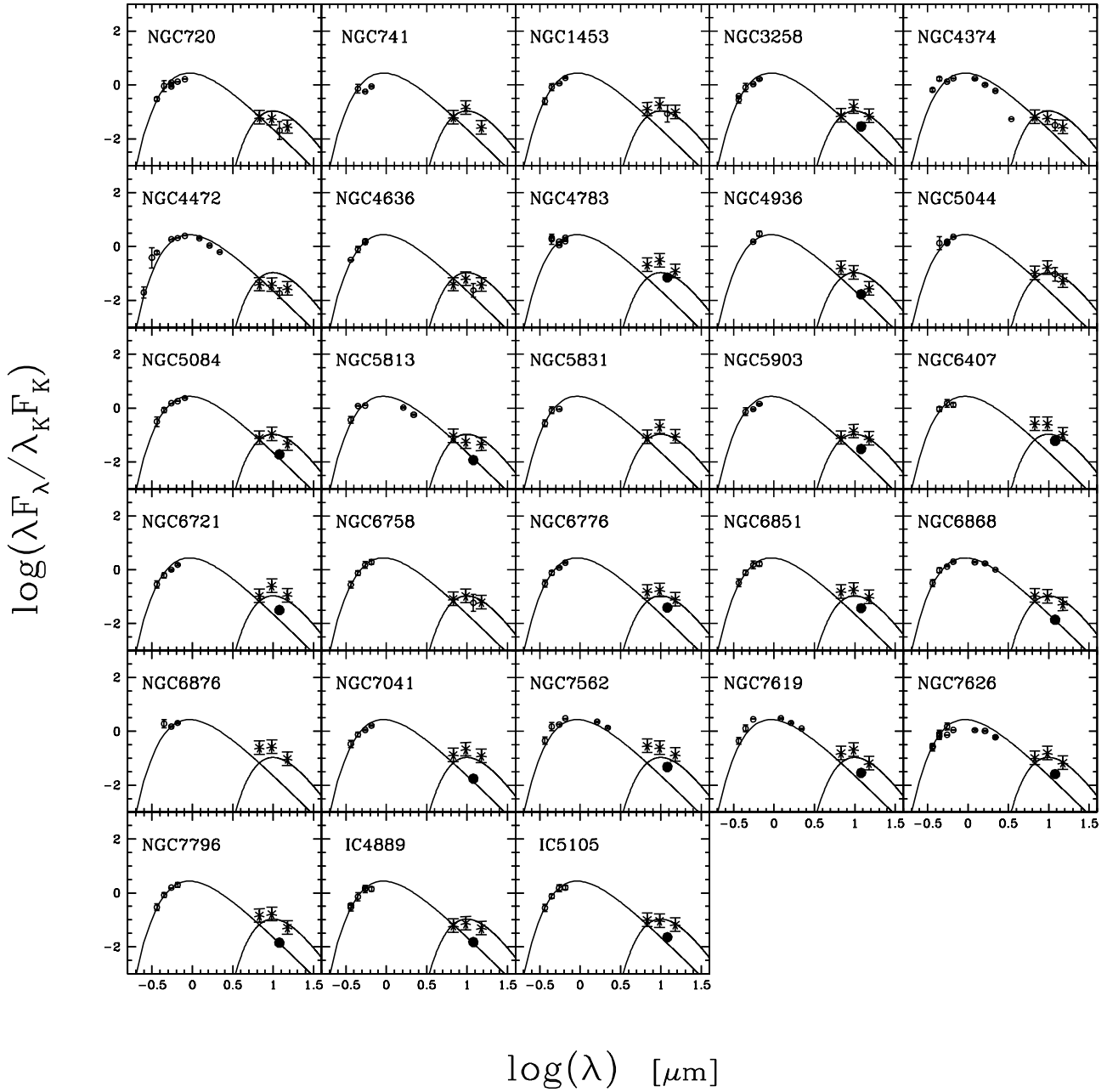


**Fig. 5.** Spectral energy distribution of the early-type galaxies in the sample. The BB corresponding to the mid-IR has a single temperature (260 K) for all galaxies.

fore use this temperature to estimate the mass of the hot dust (Section 7). In our Galaxy, the far-IR emission comes from dust heated by the interstellar radiation field (ISRF) ( $T < 22$  K) and from dust associated with O and B stars and molecular clouds ( $22\text{K} < T < 29\text{K}$ ) (Sodroski et al. 1997). In order to estimate the pure dust emission, we have subtracted, from the observed mid-IR fluxes, the underlying stellar contribution, represented by the corresponding black body curve for that galaxy group.

The typical mean stellar contributions relative to the total mid-IR fluxes ( $F_{\lambda}^* + F_{\lambda}^{\text{dust}}$ ) among the galaxy groups

are about 58% at  $6.75 \mu\text{m}$ , 22% at  $9.63 \mu\text{m}$  and 10% at  $15 \mu\text{m}$ . The infrared emission of our sample galaxies shows an appreciable contribution of the dust, a different behavior compared with the early-type galaxies in the sample of Boselli et al. (1998) or Madden et al. (1999), for example. This can be attributed to the fact that our sample was previously selected to be composed of dust-rich galaxies, therefore their emission in the IR is expected not to be purely stellar. The figures presented here use the corrected flux values.

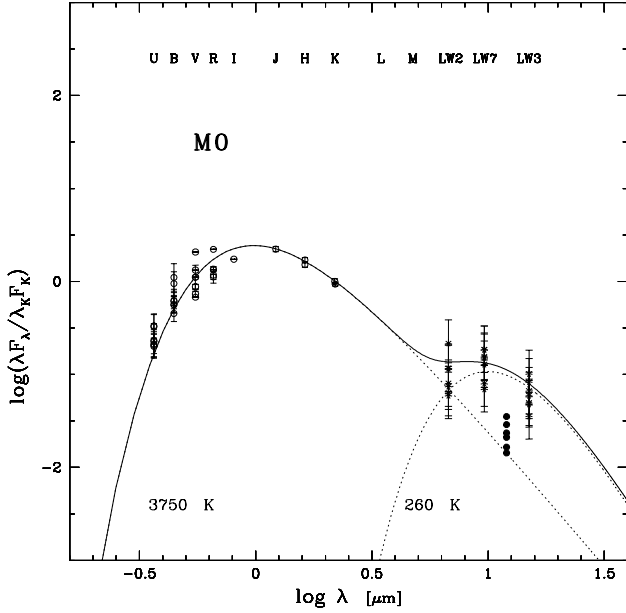


**Fig. 6.** SED for the group M0 (BB with  $T = 3750$  K) and mid-IR component with a  $T = 260$  K composite BB. Dots are NED and stars are ISO data. The black dots are IRAS ( $12\mu\text{m}$ ) upper limits.

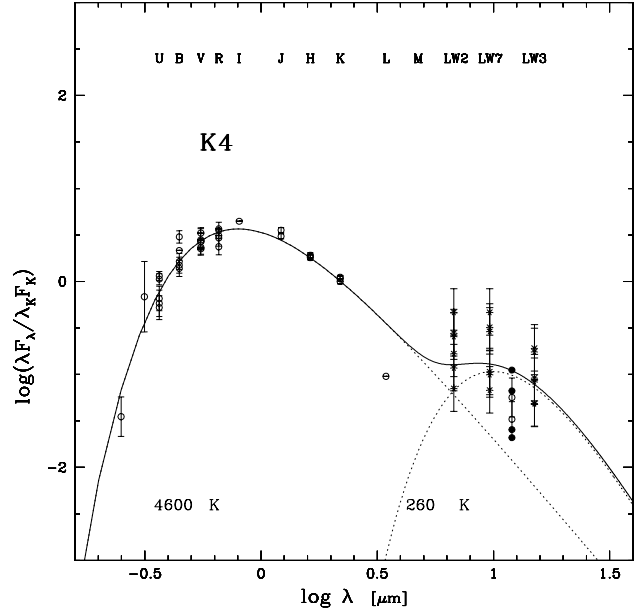


**Fig. 8.** Same as Fig 6 for the K4 galaxy group.

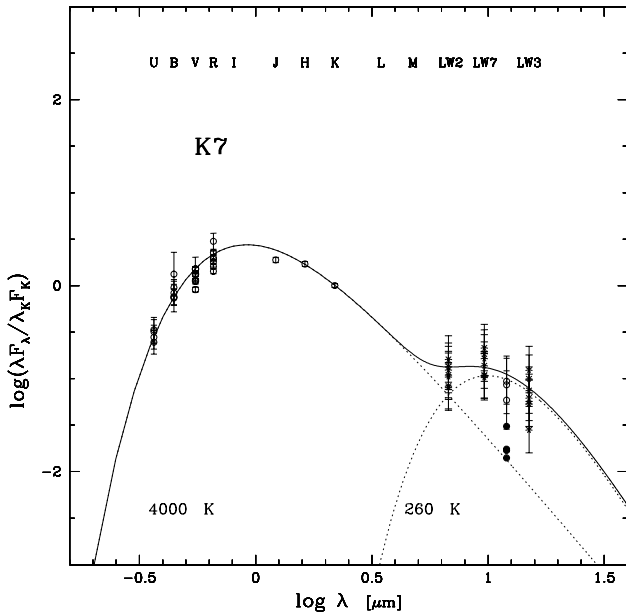


**Fig. 7.** Same as Fig 6 for the K7 galaxy group.

## 5. The mid-IR luminosity distribution

The total mid-IR luminosities (stars+dust emission) have been computed from the integrated fluxes according to:

$$L_\nu = 4\pi D^2 F_\nu \delta_\nu \quad (1)$$

Here  $\delta_\nu$  is the filter width as follows:  $\delta_{6.75\mu\text{m}} = 16.18$  THz,  $\delta_{9.63\mu\text{m}} = 6.61$  THz and  $\delta_{15\mu\text{m}} = 6.75$  THz. The fluxes  $F_\nu$

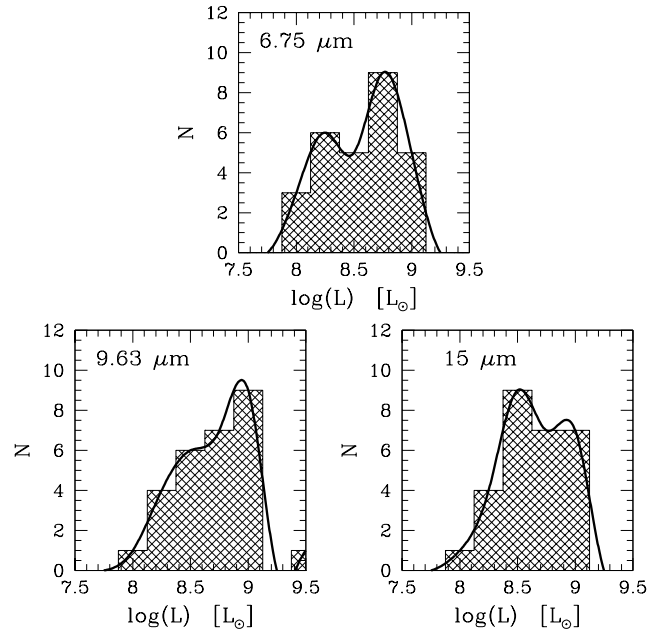


**Fig. 9.** Luminosity histograms in the three filters for sample galaxies. The solid lines correspond to a spline fit to the points.

have been integrated with an aperture corresponding to the field of view width ( $108''$ ). The luminosities are listed in Table 3, where the total mid-IR luminosity is  $L_{\text{MIR}} = L_{6.75} + L_{9.63} + L_{15}$ . The observed mid-IR luminosity ranges from  $3 - 42 \times 10^8 L_\odot$ , which is similar to what Boselli et al. (1998) found for 6 Virgo Cluster early-type galaxies.

Figure 9 shows the histograms of the luminosity distribution for the observed galaxies. The plots show the

Galaxy	$L_{6.75\mu\text{m}}$ $10^8 L_{\odot}$	$L_{9.63\mu\text{m}}$ $10^8 L_{\odot}$	$L_{15\mu\text{m}}$ $10^8 L_{\odot}$	$L_{\text{MIR}}$ $10^8 L_{\odot}$
NGC720	2.1	2.1	1.9	6.2
NGC741	9.7	23.8	8.2	41.7
NGC1453	6.7	10.9	10.7	28.3
NGC3258	2.0	4.6	3.9	10.5
NGC4374	1.0	1.0	0.8	2.7
NGC4472	1.7	1.7	2.3	5.7
NGC4636	1.3	2.3	2.5	6.1
NGC4783	7.3	11.5	8.5	27.4
NGC4936	6.4	4.7	2.2	13.4
NGC5044	3.9	6.7	4.0	14.6
NGC5084	1.7	2.5	2.1	6.3
NGC5813	2.5	1.6	2.5	6.6
NGC5831	1.2	3.1	2.5	6.8
NGC5903	2.4	4.4	4.4	11.2
NGC6407	8.8	9.5	7.2	25.5
NGC6721	4.5	11.2	9.2	24.9
NGC6758	2.9	4.1	4.4	11.5
NGC6776	9.2	11.0	9.3	29.5
NGC6851	3.2	4.0	4.0	11.3
NGC6868	5.1	5.2	4.9	15.2
NGC6876	8.8	10.2	6.7	25.7
NGC7041	2.2	3.8	4.0	10.0
NGC7562	6.1	5.7	5.7	17.5
NGC7619	5.8	8.5	4.8	19.1
NGC7626	6.3	10.2	8.2	24.7
NGC7796	5.2	6.4	3.7	15.4
IC4889	2.0	2.6	3.2	7.9
IC5105	8.8	8.9	11.6	29.3

**Table 3.** Partial and integrated total luminosities corrected by stellar contribution.

luminosities that have been corrected by subtracting the stellar component. It can be seen that the three luminosities have a similar mean value  $\log\langle L \rangle \simeq 8.6 L_{\odot}$ . The source that dominates the SED at  $6.75 \mu\text{m}$  is probably the Rayleigh-Jeans tail of the old stellar population. For  $15 \mu\text{m}$  the well defined peak at  $\log\langle L \rangle \simeq 8.5$  may indicate that for most of the galaxies in our sample the dust properties such as temperature mass and composition are similar. In order to see whether the ionizing source of the gas is also responsible for heating the dust, we studied the correlation between the mid-IR fluxes corrected by the stellar contribution and  $\text{H}\alpha$  fluxes. Figure 10 shows such a flux-flux plot, normalized by the K flux. Normalized  $6.75 \mu\text{m}$  fluxes are constant for 3 decades of  $\text{H}\alpha$ . At  $9 \mu\text{m}$  and  $15 \mu\text{m}$  the weakest  $\text{H}\alpha$  do not correlate, although for galaxies in the range  $-4.5 < \log(F_{\text{H}\alpha}/F_{\text{K}}) < -3.5$  there is a weak correlation. At least for some galaxies the source of gas ionization and dust heating must be the same and also that both gas and dust coexist in the same regions.

## 6. Mid-IR colors

The integrated properties of mid-IR dust emission in galaxies can be analysed by their colors, after subtracting the stellar population contribution. Figure 11 illus-

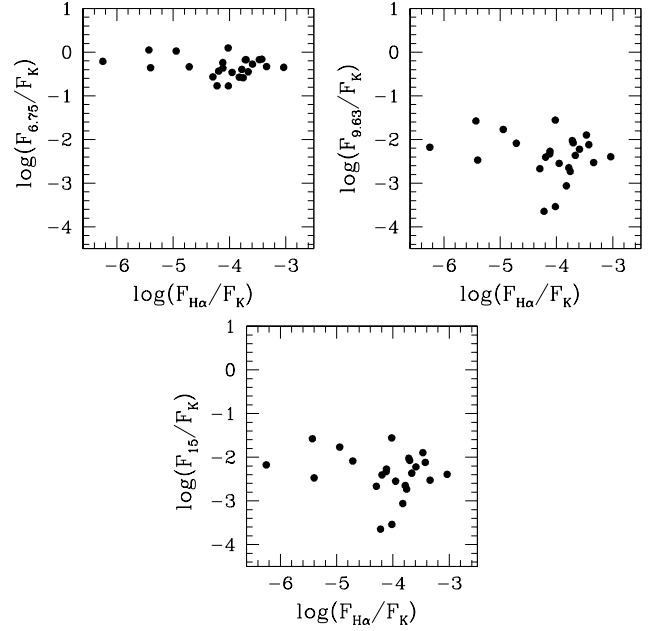


**Fig. 10.** Correlation between the mid-IR and the  $\text{H}\alpha$  luminosities. The vertical axis is the ratio between both luminosities to remove any distance effects.

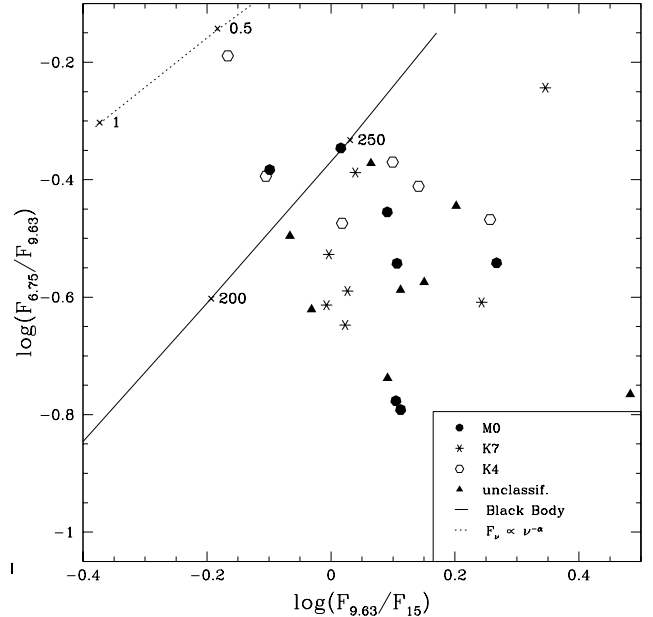


**Fig. 11.** Color-Color diagram for the sample galaxies. the line corresponds to BB at different temperatures. See text for description of the models

trates the color-color diagram for the observed  $6.75$ ,  $9.63$  and  $15 \mu\text{m}$  fluxes, along with the corresponding colors of pure black body emission for different temperatures and power-law models. Clearly, our observed  $F_{9.63}/F_{15}$  colors are bluer than those expected for a pure black body emission, concentrated near the BB with  $T = 260 \text{ K}$ . Galaxies

belonging to different stellar population groups (M0, K7, K4) can be found in the same regions of the color-color diagram. Since these colors have been obtained after subtracting the stellar population contribution they are associated to properties of the dust, such as chemical composition, optical properties, grain size and the nature of the heating source.

The blue excess of the mid-IR colors (in particular the  $F_{9.63}/F_{15}$  ratio) of our sample of galaxies with respect to the pure black body curve can be explained if we assume that the emission is produced by dust composed of graphite, silicates and PAHs, as modeled by Desert et al. (1990). This model includes three components: large silicate grains, very small graphite grains (3-dimensional) and PAHs (2-dimensional). There is a silicate band at  $9.7\mu\text{m}$ , while the main PAHs features in this spectral region are at  $3.3, 6.2, 7.7, 8.6$  and  $11.3\mu\text{m}$  (Puget, Leger and Boulanger 1985), which are covered by the filters used in the present observations. The scatter of points, for different galaxies, may be attributed to differences in the amount and/or distribution of the radiation responsible for heating the dust and PAHs. As a result, the contribution of molecules to the mid-IR emission will vary. The remaining scatter in the correlation can be easily accounted for by differences in the interstellar radiation field and dust properties.

## 7. Dust mass estimates

In the presence of a radiation field, dust grains absorb and scatter varying fractions of the incident photons, thus changing the intensity and spectral character of the radiation spectrum. Part of the absorbed energy is re-emitted in the infrared. Consequently, an analysis of the emission and absorption properties of dust grains can be used to derive estimates on the amount of dust present in galaxies.

This dust can be found in several components (Section 6), e.g. graphites, silicates, PAHs, UIBs. However, our present photometric data (broad band fluxes) do not allow us to distinguish among these components, for which it would be necessary high spectral resolution spectroscopy. Besides, recent published ISO observations and models by Athey et al. (2002) indicate that amorphous silicate are the major constituent of dust in the oxygen-rich environments in the envelopes of low mass AGB stars of early-type galaxies, where the dust is. They also have found no evidence of PAH emission in the strongest band  $7.7\mu\text{m}$  with an detection limit of 5 mJy. Accordingly, we estimate the dust mass using silicate grains as a probe; grains have similar properties, so the dust mass would not be appreciably different if we had considered graphite grains. The morphology of the ionized gas, the hot and cold dust as well as the luminosity distribution will be analyzed in detail in a paper in preparation.

A typical large dust grain absorbs photons of wavelength  $\lambda \leq 1\mu\text{m}$ , heats to a certain temperature and re-emits energy in the infrared approximately as a black-body. Our sample galaxies present a maximum in their SEDs in the mid-IR at  $\lambda \approx 10.5\mu\text{m}$  (Fig. 5), which corre-

sponds to a grain temperature  $T = 260\text{ K}$ . In the context of this paper, grains heated to that temperature are considered as hot dust. Thus, if  $L_{\text{MIR}}^g$  is an individual grain's MIR luminosity and  $L_{\text{MIR}}$  the integrated luminosity of a given galaxy observed in the range  $5\text{--}18\mu\text{m}$  (Table 3), the total number of emitting grains (hot dust) can be approximated as

$$N_{HD} \approx \frac{L_{\text{MIR}}}{L_{\text{MIR}}^g}. \quad (2)$$

A single grain luminosity is calculated using a standard emission model (Panagia 1975, Bollea and Cavaliere 1976, Barvainis 1987) in which

$$L_{\text{MIR}}^g = \int_{\nu_{\text{min}}}^{\nu_{\text{max}}} 4\pi a^2 Q_{\nu} \pi B_{\nu}(T) d\nu, \quad (3)$$

where the absorption efficiency in the infrared can be approximated by (Draine and Lee 1984)

$$Q_{\text{abs}} = 3 \frac{a}{\lambda^{1.6}} \quad (4)$$

where  $a$  and  $\lambda$  are given in  $\mu\text{m}$ .  $B_{\nu}(T)$  is Planck's black-body function and  $a$  is the grain radius. Finally, for grains with density  $\rho_g$ , the hot dust mass is

$$M_{HD} \approx \frac{4\pi}{3} a^3 N_{HD} \rho_g. \quad (5)$$

Further assumptions concerning the grain properties are necessary in order to estimate the mass are (Ferrari et al. 1999 and references therein): a) the grains are assumed to be composed mainly of silicates for which  $\rho_g = 2550\text{ kg m}^{-3}$ ; b) a single grain size is considered as a first approximation,  $a = 0.00196\mu\text{m}$ . In fact, this is the median size  $\langle a \rangle$  of a distribution  $f(a) \propto a^{-7/2}$  with  $0.0012 < a < 0.015\mu\text{m}$ ; c) a single grain temperature  $T = 260\text{ K}$  – corresponding to the hot dust component – is used and d) equation (3) is integrated between  $5 < \lambda < 18\mu\text{m}$ , since this is the range covered by the ISO filters used.

The resulting dust masses for each galaxy are shown in Table 4. We note that the masses of the hot dust component ( $T = 260\text{ K}$ ) range between  $\sim 10$  and  $\sim 200 M_{\odot}$ .

Assuming now another picture in which stars and dust are uniformly distributed throughout the galaxy, the effective extinction produced by the dust distribution on the stellar radiation field can be used to estimate the dust mass. According to this scenario, the dust luminosity ( $L_D$ ) corresponds to the absorbed fraction of the intrinsic galaxy luminosity ( $L_{\text{gal}}^*$ , assumed to come primarily from the stars), as follows:

$$\frac{L_D}{L_{\text{gal}}^*} = 1 - \frac{1 - e^{-\tau'}}{\tau'}, \quad (6)$$

$$\tau' = \frac{4}{3} \pi a^2 n_g Q_e R \quad (7)$$

where  $\tau'$  is the effective optical depth,  $n_g$  is the grain number density,  $Q_e$  is the effective absorption efficiency



**Table 4.** Dust mass

Galaxy	R	$M_{HD}$	$M_D$	$M_{AV}$
	(kpc)	( $M_\odot$ )	( $M_\odot$ )	( $10^3 M_\odot$ )
NGC 720	3.3	28	36	—
NGC 741	11.0	192	395	—
NGC 1453	7.8	130	204	—
NGC 3258	5.5	48	100	—
NGC 4374	2.0	12	10	27 <sup>†</sup>
NGC 4472	2.4	26	14	1
NGC 4636	2.4	28	18	—
NGC 4783	9.2	126	276	—
NGC 4936	6.6	62	148	—
NGC 5044	5.8	67	114	12
NGC 5084	3.4	29	45	—
NGC 5813	3.9	30	37	13
NGC 5831	3.9	31	57	—
NGC 5903	4.9	52	81	15
NGC 6407	8.9	117	200	—
NGC 6721	8.5	114	279	—
NGC 6758	6.5	53	144	4
NGC 6776	10.5	136	422	—
NGC 6851	5.4	52	73	—
NGC 6868	5.4	70	98	—
NGC 6876	7.5	118	185	—
NGC 7041	3.6	46	44	—
NGC 7562	6.8	80	178	—
NGC 7619	6.8	88	178	—
NGC 7626	6.8	114	150	—
NGC 7796	6.3	71	98	—
IC 4889	4.8	36	75	35
IC 5105	10.4	135	414	130

Table Notes. Dust masses derived from the grain luminosity ( $M_{HD}$ ), effective extinction ( $M_D$ ) and optical extinction ( $M_{AV}$ ). R is the radius of the MIR emitting region.

<sup>†</sup> Goudfrooij et al. 1994a

and  $R$  is the radius of the emitting region. We consider as a first approximation  $L_{gal}^* = L_{gal} + L_D$ . Both  $L_{gal}$  and  $L_D$  are calculated integrating the corresponding curves (Fig. 6-8) along the entire wavelength range.  $\tau'$  values are, respectively, 0.058, 0.051, 0.038 and 0.049 for the M0, K7, K4 and unclassified groups. Accordingly, the dust mass is calculated as follows:

$$M_D = \frac{4}{3}\pi R^3 n_g \frac{4}{3}\pi a^3 \rho_g = \frac{4}{3}\pi a \frac{\tau'}{Q_e} R^2 \rho_g. \quad (8)$$

The radius of the emitting regions are measured on the ISO images and are given in the second column of Table 4; grain parameters are those of silicates with  $a = 0.00196 \mu\text{m}$  and  $\rho_g = 2550 \text{ kg m}^{-3}$ . The resulting dust masses are given in Table 4. There is a good agreement between the dust mass values obtained with both methods.

Seven galaxies in the present sample are in common with the sample studied in Paper II and one with the sample of Goudfrooij et al. (1994a). For galaxies in Paper II the dust masses have been estimated from the optical extinction (which is caused mostly by cold dust  $T \sim 30 \text{ K}$

composed of big silicate grains with  $a_{si} = 0.1 \mu\text{m}$ ). These values ( $M_{AV}$ ) are shown, for comparison purposes, in the last column of Table 4. Dust masses estimated from the effective extinction are comparable to those corresponding to the hot dust, and 100 times in average smaller than those derived from the optical extinction.

We conclude that the hot dust mass component in early-type galaxies corresponds to a small fraction (a few percent) of the cold dust component. Although this is a new result for elliptical galaxies, it is not surprising since a similar effect has been observed in spiral galaxies such as M31, in which the warm dust mass, derived from the 12 and 25  $\mu\text{m}$  IRAS fluxes, is a factor  $\sim 240$  smaller than the cold dust component derived from 60 to 175  $\mu\text{m}$  fluxes (Haas et al. 1998).

## 8. Conclusions

We have shown the results of the mid-IR observation of 28 luminous early-type galaxies directed to study the properties of their interstellar medium. The sample spans a large interval in optical luminosity and includes both radio-loud and radio-quiet, X-ray emitters and non-emitters. From our observations, which consist of 6.75  $\mu\text{m}$ , 9.63  $\mu\text{m}$  and 15  $\mu\text{m}$  images, we have mapped the mid-IR dust emission and luminosities. Most of the galaxies in our sample contain extended and measurable amounts of dust in the three mid-IR wavelengths. We have built the spectral energy distribution for each galaxy from the UV to the mid-IR, and found that the SED's in the wavelength interval from the UV to the near-IR can be well matched by BB curves of temperatures  $T=3750$ ,  $T=4000$  and  $T=4600 \text{ K}$ . These temperatures correspond respectively to dominant stellar populations of spectral types M0, K7 and K4. The mid-IR data have been fitted with a composed BB with  $T=260 \text{ K}$ , for which the hot dust is a significant contributor. This curves is a reasonable fit for all the galaxies in the sample. We have estimated that the mean stellar contribution to the total mid-IR flux is about 58 % at 6.75  $\mu\text{m}$ , 22 % at 9.63  $\mu\text{m}$  and 10 % at 15  $\mu\text{m}$ . The observed mid-IR luminosity ranges from  $3 - 42 \times 10^8 L_\odot$ . We compared the mid-IR colors with the BB colors for different temperatures and showed that our observed  $F_{9.63}/F_{15}$  colors are bluer than those expected for a pure black body emission. The mid-IR colors of our sample of galaxies can be explained if we assume that the emission is the result of dust composed of graphite, silicates and PAHs as modeled by Desert et al. (1990). The dust mass of the mid-IR component was estimated assuming that the mid-IR emission comes basically from silicates grains heated at ( $T = 260 \text{ K}$ ). The mass of the hot dust component estimated in this paper ranges between 10 and 200  $M_\odot$  and we conclude that it corresponds to a very small fraction (a few percent) of the cold dust component ( $T \simeq 40 \text{ K}$ ) calculated by Merluzzi (1998) for a sample of E galaxies. Using the concept of effective optical depth, we found dust masses in the range 10 – 400  $M_\odot$ . This is in very good agreement with mass calculated from the grain luminosity. Finally, these obser-

vations have shown that in addition to gas and cold dust, the ISM of elliptical galaxies also includes a measurable amount of hot dust.

## 9. Acknowledgements

We thank M. Sauvage for providing patience assistance with the CIA packages; D. Calzetti and S. Arribas for interesting discussions and suggestions during the preparation of this work. This research has been partially supported by PRONEX/FINEP/CNPq grant 7697100300 and by the STScI visitor program.

## References

- Athey, A. E., Bregman, J. N., Bregman, J. D., Temi, P., Sauvage, M. 2002 ApJ, *in press*.  
Also [arXiv:astro-ph/0201338](https://arxiv.org/abs/astro-ph/0201338)
- Barvainis, R., 1987 ApJ, 320, 537
- Bollea, D., Cavaliere, A., 1976, A&A, 49, 313
- Boselli, B., Lequeux, J., Sauvage, M., Boulade, O., Boulanger, F., Cesarsky, D., Dupraz, C., Madden, S., Vilefond, F., 1998, A&A, 335, 53
- Caon, N., Macchetto, F.D., Pastoriza, M.G. 2000, ApJS, 127,39
- Cesarsky, D., Blommaert, J. 2000 ISOCAM Calibration Accuracies Document.  
[http://www.iso.vilspa.esa.es/manuals/CAM/accuracies/CAM\\_accur/](http://www.iso.vilspa.esa.es/manuals/CAM/accuracies/CAM_accur/)
- Desert, F.X. , Boulanger, F., and J.L. Puget 1990, A&A 237, 215
- de Vaucouleurs, G., de Vaucouleurs, A., Corwin, H. G. Jr., Buta, R. J., Paturel, G., Fouqué , P. 1991 Third Reference Catalogue of Bright Galaxies, Springer-Verlag, New York
- Draine, B. T., Lee, H. M. 1984, ApJ 285, 89
- Fabian, A.C., 1994, ARAA 32, 277
- Ferrari, F., Pastoriza, M. G., Machetto, F., Caon, N. 1999, A&AS, 136, 269
- Goudfrooij, P., Hansen, L., Jørgensen, H.E., Nørgaard-Nielsen, H.U. 1994a, A&AS, 105, 341
- Goudfrooij, P., Jong, J. de, Hansen, L., Nørgaard-Nielsen, H.U. 1994b, MNRAS , 271, 833
- Goudfrooij, P., Jong, T. de 1995, A&A, 278, 784
- Goudfrooij, P. 1995, PASP,107,502
- Haas, M., Lemke, D., Stickel, M., Hippelein, M., Kunkel, M., Herbstmeier, U., and Mattila, K., 1998, A&A, 338, L33
- Kelsall, T., Weiland, J. L., Franz, B. A., Reach, W. T., Arendt, R. G., Dwek, E., Freudenreich, H. T., Hauser, M. G., Moseley, S. H., Odegard, N. P., Silverberg, R. F., Wright, E. L. 1998, ApJ, 508, 74
- Kim, D. W. 1989 ApJ 346, 653
- Knapp, G.R., Guhathakurta, P., Kim, D.-W., Jura, M.A. 1989, ApJS, 70, 329
- Kraan-Korteweg R.C. 1986, A&A, 66, 255
- Macchetto, F., Pastoriza, M., Caon, N., Sparks, W.B., Giavalisco, M., Bender, R. , Capaccioli, M. 1996, A&AS, 120, 463 (Paper I)
- Macchetto, F 1999, Harmonizing Cosmic Distance Scale in a Post-Hipparcos Era, eds D. Egret & A. Heck, AAAP Conference Series, vol 167,217
- Madden, S.C., Vigroux, L., Sauvage, M. 1999, The Universe as seen by ISO, Eds P. Cox & M.F. Kessler, ESA-SP, 427
- Merluzzi, P. 1998 A&A, 338,807
- Natta, A., Panagia, N., 1976 A&A, 50, 191
- Panagia, N., 1975 A&A, 42, 139
- Puget J.L., Leger A., Boulanger, F., 1985, A&A, 142, L19-L22
- Sparks, W.B., Macchetto, F. Golombek D., 1989 ApJ, 345, 153
- Sodroski, T. J., Odegard, N., Arendt, R. G., Dwek, E., Weiland, J. L., Hauser, M. G., Kelsall, T 1997, ApJ, 480, 173.
- Van Dokkun, P.G., Franx, M. 1995, ApJ, 110, 2027